

Is ozone a reliable proxy for molecular oxygen?

II. The impact of N₂O on the O₂-O₃ relationship for Earth-like atmospheres

Thea Kozakis^{1,2,*}, João M. Mendonça^{1,3,4}, Lars A. Buchhave¹, and Luisa M. Lara²

- National Space Institute, Technical University of Denmark, Elektrovej, 2800 Kgs. Lyngby, Denmark
- ² Instituto de Astrofísica de Andalucía CSIC, Glorieta de la Astronomía s/n, 18008 Granada, Spain
- ³ School of Physics and Astronomy, University of Southampton, Highfield, Southampton SO17 1BJ, UK
- ⁴ School of Ocean and Earth Science, University of Southampton, Southampton SO14 3ZH, UK

Received 24 April 2025 / Accepted 27 May 2025

ABSTRACT

Molecular oxygen (O_2) will be an important molecule in the search for biosignatures in terrestrial planetary atmospheres in the coming decades. In particular, O_2 combined with a reducing gas (e.g., methane) is considered strong evidence for disequilibrium caused by surface life. However, there are circumstances where it would be very difficult or impossible to detect O_2 , in which case it has been suggested that ozone (O_3) , the photochemical product of O_2 , could be used instead. Unfortunately, the O_2 - O_3 relationship is highly nonlinear and dependent on the host star, as shown in detail in the first paper of this series. This paper further explores the O_2 - O_3 relationship around GOV-M5V host stars, using climate and photochemistry modeling to simulate atmospheres while varying abundances of O_2 and nitrous oxide (N_2O) . Nitrous oxide is of particular importance to the O_2 - O_3 relationship not only because it is produced biologically, but because it is the primary source of nitrogen oxides (NO_x) , which fuel the NO_x catalytic cycle, which destroys O_3 and the smog mechanism that produces O_3 . In our models we varied the O_2 mixing ratio from 0.01-150% of the present atmospheric level (PAL) and N_2O abundances of 10% and 1000% PAL. We find that varying N_2O impacts the O_2 - O_3 relationship differently depending strongly on both the host star and the amount of atmospheric O_2 . Planets orbiting hotter hosts with strong UV fluxes efficiently convert N_2O into NO_x , often depleting a significant amount of O_3 via faster NO_x catalytic cycles. However, for cooler hosts and low O_2 levels we find that increasing N_2O can lead to an increase in overall O_3 due to the smog mechanism producing O_3 in the lower atmosphere. Variations in O_3 result in significant changes in the amount of harmful UV reaching the surfaces of the model planets as well as the strength of the $9.6 \ \mu m$ O_3 emission spectral feature, demonstrating potent

Key words. astrobiology – planets and satellites: atmospheres – planets and satellites: terrestrial planets – planetary systems

1. Introduction

Numerous studies have suggested the use of ozone (O₃) as a proxy for molecular oxygen (O2) in recent decades (e.g., Léger et al. 1993; Des Marais et al. 2002; Segura et al. 2003; Léger et al. 2011; Meadows et al. 2018b). This is largely because O₂ when combined with a reducing species such as methane (CH₄), is considered a strong disequilibrium biosignature. Observing both in a terrestrial planetary atmosphere indicates that strong replenishing fluxes of O₂ and CH₄ must be present. Currently, life is the only known mechanism capable of providing these replenishing fluxes (e.g., Lovelock 1965; Lederberg 1965; Lippincott et al. 1967; Meadows 2017). Ozone comes into the picture because there are scenarios in which O2 would be very difficult or impossible to detect in a planetary atmosphere when O₃ is readily detectable. For example, the mid-IR is an excellent wavelength range for atmospheric characterization, due to the strong spectral features of potential biosignatures (e.g., Quanz et al. 2022; Angerhausen et al. 2024) along with the lessened impact of clouds in planetary emission spectra (e.g., Kitzmann et al. 2011). However, there are no strong O₂ features in the mid-IR – only a collisionally induced absorption feature, which is sensitive only to large amounts of abiotically produced O2, not to the smaller amounts indicative of life (Fauchez et al. 2020). Another

example considers a planetary atmosphere resembling the low O_2 environment of early Earth, rather than the oxygen-rich atmosphere of modern Earth (O_2 comprising 21% of the atmosphere). Observing a planet with O_2 abundances expected from the Proterozoic era on Earth (2.4–0.54 Gyr ago) O_2 would be difficult to detect, while O_3 may be detected at trace amounts (e.g., Kasting et al. 1985; Léger et al. 1993; Des Marais et al. 2002; Segura et al. 2003; Léger et al. 2011). For these reasons O_3 has been seen as a good alternative to O_2 .

However, although O_3 is the photochemical product of O_2 , it has also been known for decades that the O₂-O₃ relationship is highly nonlinear, due to both the pressure and temperature dependency of O₃ formation and the requirement of UV for O₂ photolysis. To study this further, in the previous paper of this series, Kozakis et al. (2022), we performed atmospheric modeling of Earth-like planets for a range of O₂ abundances and a variety of host stars. Here, we use the term "Earth-like" to refer to a terrestrial planet that is the same size and density as Earth, possesses a similar atmospheric composition, and orbits at a distance where it receives the same total flux from its host star as modern Earth. In our first study, we varied the atmospheric abundance of O₂ from 0.01-150% PAL (present atmospheric level) around G0V-M5V host stars. We found that the O2-O3 relationship was extremely influenced by the host star, with planets around hotter stars (G0V-K2V) following different trends

^{*} Corresponding author.

to those around cooler stars (K5V-M5V). Planets around hotter stars reached their peak O₃ abundance at O₂ levels of just 25-55% PAL, with the Earth-Sun system having a similar amount of O₃ at both 10% and 100% PAL O₂. This was due to the pressure dependency of O₃ formation, an effect first discussed in Ratner & Walker (1972), although our previous study was the first to replicate it using modern atmospheric models and host stars other than the Sun. Cooler stars, on the other hand, were shown to host planets on which O_3 decreased along with O_2 . Additionally, we found that the amount of UV reaching the planetary surface varied nonlinearly with both incoming UV and O₃, and that O₃ features in simulated emission spectra depended more strongly on atmospheric temperature profiles than on the actual amount of O₃ (or O₂) in the atmosphere. Already from that study, we determined that using O₃ as a proxy for O₂ would require knowledge of the host star spectrum, climate and photochemistry modeling, and general atmospheric context. For planets around hotter hosts, another layer of complexity exists, due to the fact that similar O₃ abundances can occur at very different O₂ values, making it impossible to glean the total O₂ abundance from a measurement of only total O₃ abundance. However, O₃ measurements could still provide useful information on the atmosphere and potentially give insight into whether life could exist on the planetary surface. This paper is a continuation of that study, specifically focusing on how O2-O3 relationships could vary with different atmospheric compositions.

In this current study, we expand upon the models from Kozakis et al. (2022) by varying not only O_2 but also nitrous oxide (N_2O). Nitrous oxide is particularly interesting in this context, not only because it is biologically produced and considered a promising biosignature (e.g., Schwieterman et al. 2018; Angerhausen et al. 2024), but also because it is the "parent species" of nitrogen oxides (NO_x). These nitrogen oxides play a crucial role in the two catalytic cycles that destroy O_3 as well as the smog mechanism that produces O_3 .

Since the rate at which N_2O is converted into NO_x is dependent on photolysis rates, the degree to which varying N_2O impacts the O_2 - O_3 relationship depends on both the overall spectrum of the host star as well as the UV spectral slope. This paper includes all of the models from Kozakis et al. (2022), rerun with different amounts of N_2O . Section 2 reviews the relevant chemistry of O_3 and N_2O , and Sect. 3 describes the atmospheric models, the input stellar spectra, and the radiative transfer model. Section 4 analyzes how varying N_2O alters atmospheric chemistry, surface UV flux, and simulated planetary emission spectra. Section 5 compares this to similar studies and discusses atmospheric parameters, which affect N_2O abundances in Earth-like planetary atmospheres. A summary of the study and conclusions are available in Sect. 6.

2. Relevant chemistry

2.1. Ozone formation and destruction

The majority of O_3 on Earth is formed via the Chapman mechanism (Chapman 1930), beginning with O_2 photolysis creating atomic O, which then combines with another O_2 molecule with the help of a background molecule, M, to carry away the excess energy:

$$O_2 + h\nu \to O + O (175 < \lambda < 242 \text{ nm}),$$
 (1)

$$O + O_2 + M \rightarrow O_3 + M. \tag{2}$$

Since Reaction (2) is a three-body reaction, it proceeds faster at higher atmospheric densities, with this reaction in particular having a strong temperature dependence, favoring cooling temperatures. While Reaction (1) creates ground state O atoms (also written as $O(^3P)$), the O_2 photolysis initiated by photons with wavelengths less than 175 nm creates the $O(^1D)$ radical,

$$O_2 + h\nu \to O + O(^1D) (\lambda < 175 \text{ nm}),$$
 (3)

which can then be quenched back to the ground state via collisions with a background molecule,

$$O(^{1}D) + M \to O + M, \tag{4}$$

or react with other molecules. Similarly O_3 photolysis creates O_2 and either a ground O atom or an excited $O(^1D)$ radical depending on the energy level of the photon:

$$O_3 + h\nu \rightarrow O_2 + O(^1D)(\lambda < 310 \text{ nm}),$$
 (5)

$$O_3 + h\nu \rightarrow O_2 + O (310 < \lambda < 1140 \text{ nm}).$$
 (6)

After photolysis the resulting O atom often recombines with O_2 via Reaction (2), so the photolysis of O_3 is not seen as a loss of O_3 . Due to the constant cycling between O_3 and O_3 , it is often useful to keep track of O_3 , termed "odd oxygen", rather than tracking both individually. Odd oxygen can be lost when converted to O_2 molecules, as seen in,

$$O_3 + O \rightarrow 2O_2. \tag{7}$$

The conversion of odd oxygen back into O_2 requires the Chapman mechanism to restart with O_2 photolysis, which is the slowest and limiting reaction of O_3 formation. However, Reaction (7) is significantly slower, so O from O_3 photolysis tends to preferentially combine with O_2 back into O_3 (Reaction (2)). On Earth the majority of O_3 is created via the Chapman mechanism, with formation rates highest in the stratosphere. This region is high enough in the atmosphere that O_2 is quickly photolyzed, yet still has sufficient atmospheric density for the three-body reaction that creates O_3 (Reaction (2)) to be efficient.

Lower in the atmosphere, primarily in the troposphere, there is another mechanism for O₃ formation, which is referred to as "smog formation" (Haagen-Smit 1952), expressed as,

$$OH + CO \rightarrow H + CO_2, \tag{8}$$

$$H + O_2 + M \rightarrow HO_2 + M, \tag{9}$$

$$HO_2 + NO \rightarrow OH + NO_2,$$
 (10)

$$NO_2 + h\nu \to NO + O, \tag{11}$$

$$O + O_2 + M \rightarrow O_3 + M. \tag{2}$$

Net:
$$CO + 2O_2 + h\nu \rightarrow CO_2 + O_3$$

This chain of reactions requires hydrogen oxides (HO_x , HO_2 $\tilde{+}$ OH + H) and nitrogen oxides (NO_x , NO_3 + NO_2 + NO_3 as catalysts, although they are not consumed. On Earth the smog mechanism is slower and produces significantly less O_3 than the Chapman mechanism, but studies such as Grenfell et al. (2013) have demonstrated that planets around cooler spectral hosts may experience much higher efficiency in the smog mechanism.

While the Chapman and smog mechanisms are the main sources of O₃ formation, catalytic cycles are the main sources

of O₃ destruction. These are cycles in which there is a net loss of odd oxygen as follows,

$$\begin{array}{c} X + O_3 \rightarrow XO + O_2, \\ XO + O \rightarrow X + O_2, \\ \hline \text{Net:} \quad O_3 + O \rightarrow 2O_2 \end{array}$$

with X and XO cycling between each other without loss. On Earth the two most dominant cycles use X = NO and X = OH for the NO_x and HO_x catalytic cycles, respectively. The HO_x catalytic cycle is as follows,

$$OH + O_3 \rightarrow HO_2 + O_2, \tag{12}$$

$$HO_2 + O \rightarrow OH + O_2,$$
 (13)

in which odd oxygen, $O + O_3$, is converted into two O_2 . In the upper stratosphere where H atoms are more common (often from H_2O photolysis) odd oxygen can be converted to O_2 via,

$$H + O_2 + M \rightarrow HO_2 + M, \tag{14}$$

$$HO_2 + O \rightarrow OH + O_2,$$
 (13)

$$OH + O \rightarrow H + O. \tag{15}$$

In the lower stratosphere where there is less O_2 photolysis and therefore fewer O atoms, odd oxygen is destroyed via,

$$OH + O_3 \rightarrow HO_2 + O_2, \tag{16}$$

$$HO_2 + O_3 \to OH + 2O_2.$$
 (17)

There are multiple reactions that destroy either OH or HO_2 , but they are typically recycled back into another HO_x species. Photolysis is also not a true sink of HO_x , since HO_2 photolysis creates OH, and OH is too short-lived for significant photolysis. Efficient methods of HO_x destruction include conversion to H_2O ,

$$OH + HO_2 \rightarrow H_2O + O_2, \tag{18}$$

or conversion to a stable reservoir species, such as

$$OH + OH + M \rightarrow H_2O_2 + M, \tag{19}$$

$$OH + NO_2 + M \rightarrow HNO_3 + M, \tag{20}$$

$$HO_2 + NO_2 + M \rightarrow HO_2NO_2 + M. \tag{21}$$

The other primary catalytic cycle, the NO_x catalytic cycle, is discussed in the next subsection, as it is fueled by N_2O .

2.2. Nitrous oxide and NOx catalytic cycles

Nitrous oxide, considered itself a biosignature, is primarily created by nitrification and denitrification processes in soils and oceans, with very few abiotic sources. On Earth there are additionally many anthropogenic sources of N_2O , mainly from agricultural processes. The only known major sink of N_2O is photolysis in the stratosphere. N_2O photolysis is one of the sources of the $O(^1D)$ radical,

$$N_2O + h\nu \to N_2 + O(^1D),$$
 (22)

which can react with N₂O to create NO,

$$N_2O + O(^1D) \rightarrow NO + NO,$$
 (23)

or N_2 and O_2 ,

$$N_2O + O(^1D) \to N_2 + O_2.$$
 (24)

While N_2O is the main non-anthropogenic source of NO_x , there are additionally minor sources of NO_x from cosmic rays and lightning (e.g., Nicolet 1975; Tuck 1976; Shumilov et al. 2003; Braam et al. 2022), which are not explored in this study. The primary NO_x catalytic cycle working in the stratosphere follows as,

$$NO + O_3 \rightarrow NO_2 + O_2, \tag{25}$$

$$NO_2 + O \rightarrow NO + O_2. \tag{26}$$

Nitrate (NO_3) is photolyzed at longer wavelengths, allowing NO_3 photolysis to occur in the lower stratosphere and further contributing to O_3 destruction, as follows,

$$NO + O_3 \rightarrow NO_2 + O_2, \tag{25}$$

$$NO_2 + O_3 \rightarrow NO_3 + O_2,$$
 (27)

$$NO_3 + h\nu \to NO + O_2. \tag{28}$$

 NO_x is lost from the atmosphere through reactions with N atoms, as shown below,

$$NO + N \rightarrow N_2 + O, \tag{29}$$

where the N atoms are produced by the photolysis of NO:

$$NO + h\nu \rightarrow N_2 + O. \tag{30}$$

Other sinks include conversion to reservoir species, as shown by

$$NO_2 + NO_3 + M \to N_2O_5 + M,$$
 (31)

$$OH + NO_2 + M \rightarrow HNO_3 + M, \tag{20}$$

$$HO_2 + NO_2 + M \rightarrow HO_2NO_2 + M, \tag{21}$$

in which the reservoir species are significantly less reactive.

2.3. NO_x-limited and NO_x-saturated regimes

Since the smog mechanism uses O atoms created by NO_2 photolysis to create O_3 , it might seem that an increase in NO_x in the lower atmosphere would always lead to a faster smog mechanism. However, the relationship between NO_x and the smog mechanism is complicated due to the relationship between NO_x and HO_x . While NO_x is produced from N_2O in the atmosphere, HO_x is often indirectly created from O_3 itself. Hydroxyl (OH) is most commonly created by oxidation of water with the $O(^1D)$ radical,

$$H_2O + O(^1D) \to OH + OH,$$
 (32)

with the majority of $O(^{1}D)$ in the lower atmosphere created from O₃ photolysis (Reaction (5)). Therefore, an increase in O₃ often leads to an increase in HO_x . It follows that an increase in NO_x would allow increased smog production of O₃, with the higher O_3 concentrations creating more HO_x . However, this only holds true in what we call a "NO_x-limited" regime, where increasing NO_x leads to an increase in HO_x . Sufficiently high levels of NO_x will induce a shift into what we call the " NO_x -saturated" regime, where NO_x will become efficient at locking up HO_x into reservoir species such as HNO3 and HO2NO2 (Reactions (20) and (21)). This relationship in the NO_x -limited and NO_x -saturated regimes as they exist for modern Earth is shown in Fig. 1. Since NO_x and HO_x are primarily created through reactions of $O(^1D)$ with N_2O and H_2O , respectively (Reactions (23,32)), and $O(^1D)$ is created via photolysis, the amount of incoming UV from the host star plays a crucial role in determining which NO_x regime is dominant in the atmosphere.

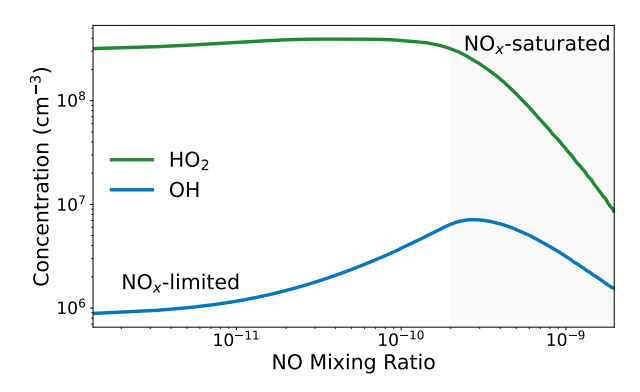


Fig. 1. Impact of HO_2 and OH in the NO_x -limited and NO_x -saturated regimes on modern Earth, adapted from Logan et al. (1981). In the NO_x -limited regime (white background), increasing NO_x allows for a more efficient smog mechanism, with the resulting increase in O_3 causing a corresponding rise in HO_x . In the NO_x -saturated regime (gray background), the abundance of NO_x rises to the point where smog O_3 production is suppressed as NO_x depletes HO_x (a necessary catalyst for the smog mechanism) by locking it up into reservoir species.

3. Methods

3.1. Atmospheric models

We used Atmos¹, a publicly available 1D coupled climate and photochemistry code for atmospheric modeling, following Kozakis et al. (2022). Here, we give a brief summary of the code, with more details available in other papers (Arney et al. 2016; Meadows et al. 2018a; Kozakis et al. 2022). For inputs Atmos requires a stellar host spectrum (121.6–45 450 nm), upper and lower boundary conditions for individual gases, initial concentrations of gaseous species, and planetary parameters (radius, gravity, and surface albedo).

We used the modern Earth template for the photochemistry code (Kasting 1979; Zahnle et al. 2006), which contains 50 gaseous species and a network of 233 chemical reactions. The atmosphere was calculated up to 100 km and was broken up into 200 plane parallel layers, each solving the flux and continuity equations simultaneously to determine the atmospheric composition. Vertical transport was included for all the species that were not considered "short-lived," including molecular and eddy diffusion. Radiative transfer calculations used the δ -2-stream method developed in Toon et al. (1989), and convergence was reached when the adaptive time step reached the age of the universe (\sim 10¹⁷ seconds) within the first 100 steps of the code.

The climate model (Kasting & Ackerman 1986; Kopparapu et al. 2013; Arney et al. 2016) calculates the temperature and pressure profile of the atmosphere based on the incoming stellar radiation and the atmospheric composition. As with the photochemistry code, a δ -2-stream multiple scattering method computes the absorption of stellar flux throughout the atmosphere, and then a correlated-k method computes the absorption of O₃, H₂O, CH₄, CO₂, and C₂H₆ in each layer for outgoing IR radiation including both single and multiple scattering. The atmosphere was broken up into 100 layers from the surface up until 1 mbar (typically <60–70 km), as the code could not be reliably run above these pressures (Arney et al. 2016). Temperatures and species profiles were held constant above this altitude when transferred to the photochemistry code. Convergence was achieved when the temperature and flux differences out of the

Table 1. Model parameters.

Model name	N ₂ O MR	O ₂ MR
Kozakis et al. (2022)	3.0×10^{-7}	$2.1 \times 10^{-5} - 0.315$
Low N ₂ O (10% PAL)	3.0×10^{-8}	$2.1 \times 10^{-5} - 0.315$
High N ₂ O (1000% PAL)	3.0×10^{-6}	$2.1 \times 10^{-5} - 0.315$

Notes. Abbreviations: MR = mixing ratio; PAL = present atmospheric level.

top of the atmosphere were deemed sufficiently small ($<10^{-5}$) (Arney et al. 2016).

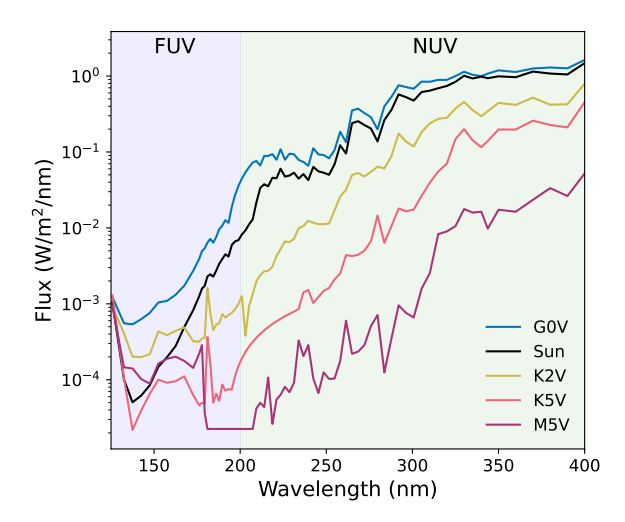
We ran the climate and photochemistry models, coupled using the "short-stepping" convergence method (Teal et al. 2022; Kozakis et al. 2022), iterating back and forth for 30 iterations or until convergence for the two codes was reached. For this study we explored "Earth-like" atmospheres around a variety of host stars, with varying constant mixing ratios of O₂ and N₂O, building off of Kozakis et al. (2022), who modeled only variations in O_2 . As in Kozakis et al. (2022) we used modern Earth initial conditions for our model atmospheres and varied O₂ from 0.01– 150% PAL. Lower O₂ values were not explored because they are likely unstable Gregory et al. (2021), and higher values similarly were not explored as they are not compatible with life due to O₂ combustibility (Kump 2008). All our model planets were run at the Earth-equivalent distance, with a surface pressure of 1 bar, the radius of Earth, and initial gaseous species abundances as listed in the modern Earth Atmos template. This study used all the models from Kozakis et al. (2022) with high and low N₂O models using 1000 and 10% PAL N₂O, respectively (see Table 1). Fixed mixing ratios of N₂O were used (with the modern value of $N_2O=3.0 \times 10^{-7}$), to better isolate the effects on O₃. These values were picked in order to begin mapping out the parameter space of atmospheres with different biological fluxes and their impact on O₃ at different O₂ levels. Since we delved into the O2-O3 relationship for changing only O2 in Kozakis et al. (2022), this paper primarily focuses on how changes in N₂O impact O₃ levels and the atmosphere generally in comparison to the models with modern levels of N_2O .

3.2. Input stellar spectra

The same Atmos input stellar spectra from Kozakis et al. (2022) were used, with hosts ranging from G0V-M5V (for more details, see Kozakis et al. 2022). The G0V-K5V stellar spectra were originally created in Rugheimer et al. (2015) and consist of UV data from International Ultraviolet Explorer (IUE) data archives² combined with ATLAS spectra (Kurucz 1979) for the visible and IR wavelength regions. For the M5V star, we used UV data of GJ 876 from the Measurements of the Ultraviolet Spectral Characteristics of Low-mass Exoplanetary Eystems (MUSCLES) survey (France et al. 2016). The UV spectra of all host stars are shown in Fig. 2 along with a comparison to cross sections of gaseous species relevant to O₃ formation and destruction. The UV spectrum is important for O₃ formation, particularly the UV spectral slope of the far-UV (FUV; λ < 200 nm) and mid- and near-UV (abbreviated NUV, for brevity; 200 nm $< \lambda < 400$ nm), with later stars tending to have higher FUV/NUV ratios due to activity and high NUV absorption via TiO (Harman et al. 2015).

https://github.com/VirtualPlanetaryLaboratory/atmos

http://archive.stsci.edu/iue



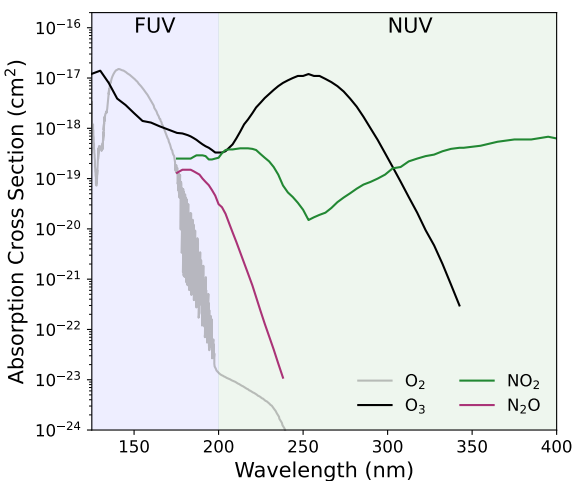


Fig. 2. UV stellar spectra of the host stars in this study (top) and corresponding absorption cross sections of relevant gaseous species (bottom). The two plots cover the same wavelength range in order to facilitate comparisons. Cross sections for NO_2 and N_2O are cut off at shorter wavelengths, due to the dominance of absorption from CO_2 and other atmospheric species.

3.3. Post-processing radiative transfer models

We used the Planetary Intensity Code for Atmospheric Scattering Observations (PICASO) to compute planetary emission spectra from our atmospheric models (Batalha et al. 2019, 2021), following Kozakis et al. (2022). This code is publicly available with the ability to compute transmission, reflectance, and emission spectra. For emission spectra we input atmospheric profiles of gaseous species and T/P profiles from Atmos and run our models at a phase angle 0° (full phase) for wavelengths of $0.3{\text -}14~\mu\text{m}$. We focus in particular on the $9.6~\mu\text{m}$ O_3 feature.

4. Results

Here, we explore the results of our planetary atmospheric models for high and low N_2O and compare them to the Kozakis et al. (2022) atmospheric models with modern levels of N_2O . The impact of varying N_2O levels on the O_2 - O_3 relationship is shown to be nonlinear in all cases, with a strong dependency on both the stellar host and the amount of atmospheric O_2 . In Sect. 4.1 we analyze the atmospheric chemistry of the varying

 N_2O models, the variations in UV to the ground in Sect. 4.2, and the resulting planetary emission spectra in Sect. 4.3. Additional supporting figures and tables are available in Appendix A.

4.1. Atmospheric chemistry

4.1.1. Atmospheric chemistry: Overview

Changing N₂O is shown to have varying effects on the O₂-O₃ relationship depending on the O₂ level and stellar host, with stronger effects seen with high N2O models when compared to the low N2O models. Results for O3 abundances normalized to modern levels of N2O with the high and low N2O models at 100%, 10%, 1%, and 0.1% PAL O₂ for all hosts are in Fig. 3, with absolute O3 values for all O2 levels modeled for the Sunand M5V-hosted planets in Fig. 4. Absolute O3 results for planets around all hosts at all modeled N2O and O2 levels with a comparison to results from Kozakis et al. (2022) are located in the Appendix (Fig. A.1). For planets around all hosts at O₂ levels near 100% PAL there is a decrease in O₃ for high N₂O, and an increase in O₃ for low N₂O. Planets hosted by all stars except the coolest one (M5V) experience a large amount of O₃ depletion at O2 levels similar to modern Earth for the high N2O models, with K2V having the overall largest depletion at 100% PAL, only retaining 47% of its O₃ when compared to models with modern levels of N2O. In contrast for the corresponding model for the M5V-hosted planet 95% of the original O₃ remains.

For the low N_2O models at 100% PAL O_2 the planets around both the Sun and the K2V host are most impacted, with O_3 abundances of 129% of the O_3 they had with modern N_2O levels. Again, the planet around the M5V host is least affected, with 103% of the O_3 compared to results from modern N_2O levels. At low O_2 levels for the high N_2O models planets around all hosts experience an increase in O_3 , with this effect being most significant for the planet around the M5V host. The main factors at work determining the impact of N_2O on O_3 abundance are:

- the balance between the host star's ability to convert N₂O into NO_x and to destroy N₂O via photolysis
- whether the amount of NO_x reaches the threshold to enter the NO_x-saturated regime, which inhibits the smog mechanism
 Both of these concepts are discussed at length in the following subsections.

4.1.2. Atmospheric chemistry: Efficiency of conversion of N₂O into NO_x and N₂O photolysis

The degree to which varying N_2O impacts O_3 abundance is largely dependent on the host stars' ability to convert N_2O into NO_x , as well as the rate at which N_2O is destroyed via photolysis. Although N_2O levels are the same for planets around all host stars, the rate at which the incoming host star flux converts N_2O to NO_x varies based on the UV spectrum of the host. Conversion of N_2O into NO_x requires an $O(^1D)$ radical (Reaction (23)), which is created via,

$$O_2 + h\nu \to O + O(^1D) (\lambda < 175 \text{ nm}),$$
 (3)

$$O_3 + h\nu \rightarrow O_2 + O(^1D) (\lambda < 310 \text{ nm}),$$
 (5)

$$N_2O + h\nu \to N_2 + O(^1D) (\lambda < 200 \text{ nm}),$$
 (33)

$$CO_2 + h\nu \to CO + O(^1D) (\lambda < 167 \text{ nm}).$$
 (34)

As all of these reactions require short-wavelength UV photons, naturally planets with hotter hosts and higher UV fluxes are

https://natashabatalha.github.io/picaso/index.html

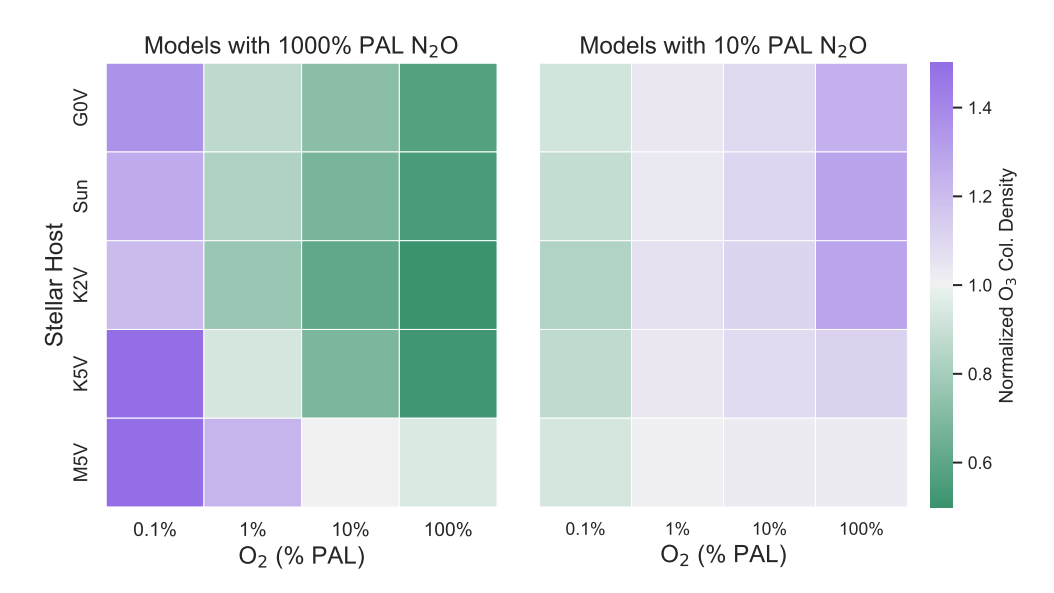


Fig. 3. Total O_3 abundances for models with high N_2O (left) and low N_2O (right) normalized to models with modern levels of N_2O from Kozakis et al. (2022). Overall, the high N_2O models impacted the O_2 - O_3 relationship more than the low N_2O models, with the results being highly dependent on the stellar host and the amount of O_2 . High N_2O models with hotter stars experience significant O_3 depletion due to faster NO_x catalytic cycles caused by increased N_2O . However, for the high N_2O models at very low O_2 levels, planets around all the hosts experience an increase in O_3 due to the higher efficiency of the smog mechanism once the Chapman mechanism is limited by low amounts of O_2 . The M5V-hosted planet in particular experiences an increase in O_3 with the high N_2O models beginning at 10% PAL O_2 and lower, due to the increased capabilities of the smog mechanism in this lower UV environment.

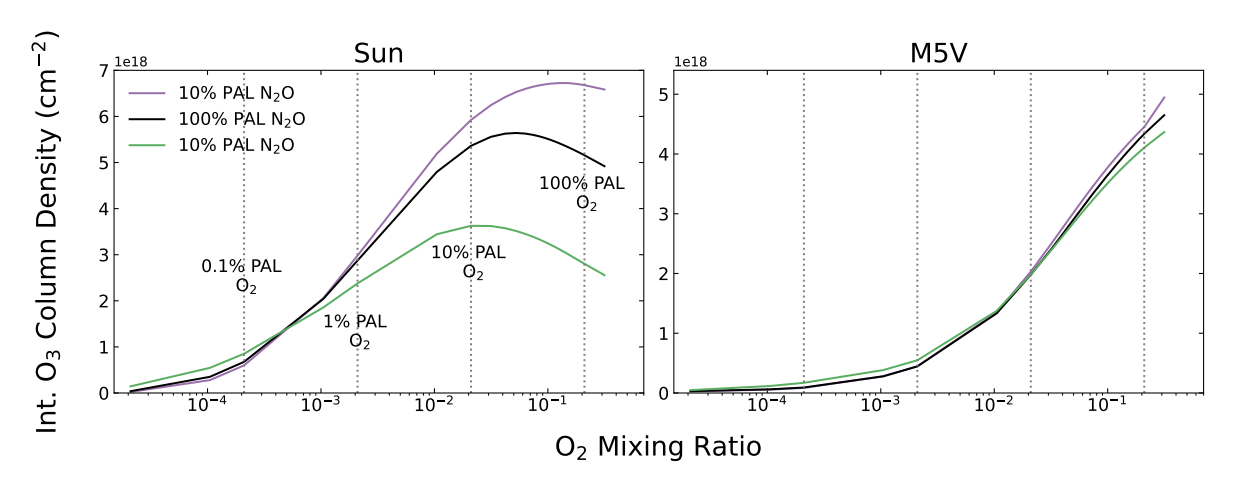


Fig. 4. O_2 - O_3 relationship with high, low, and modern N_2O models for planets around the Sun and M5V hosts. Vertical dashed lines indicate O_2 levels of 100%, 10%, 1%, and 0.1% PAL. The phenomena causing maximum O_3 production for the planet around the Sun to occur at O_2 values less than the maximum O_2 value modeled are explained in depth in Kozakis et al. (2022). In general, the M5V-hosted planet experiences significantly less variation in O_3 for different N_2O abundances than the Sun-hosted planet because the low UV flux of the M5V host is not as efficient at converting N_2O into NO_x as other hosts with higher UV fluxes. O_2 - O_3 relationships for planets around all hosts and comparisons to Kozakis et al. (2022) are in Figure A.1.

more efficient at creating $O(^1D)$, and therefore at converting N_2O into NO_x . However, the high UV fluxes of these hosts also destroy significant amounts of N_2O via photolysis – the main sink of N_2O . This depletion of N_2O via photolysis becomes even more significant for lower O_2 levels, as photolysis in general can occur deeper in the atmosphere when there is less UV shielding from O_2 and O_3 . This effect is discussed at length in Kozakis et al. (2022). The end result is that although the GOV and Sun hosts are most efficient at converting N_2O into NO_x , the high levels of N_2O destruction from photolysis mean that NO_x production is hindered, especially at low O_2 levels, due to the loss of the source N_2O . The host star displaying the largest increase in NO_x with the high N_2O models is the K2V host, as

it exists in a "sweet spot" where the UV flux is capable of creating enough $O(^1D)$ to fuel conversion of N_2O into NO_x , but not enough UV for significant N_2O depletion to hinder NO_x production. Planets around the M5V host show the least variation in NO_x production when varying N_2O , due to low incoming UV flux.

When varying N_2O the amount of NO_x created is the main driver of stratospheric O_3 destruction via the NO_x catalytic cycle, resulting in overall depletion of O_3 for high N_2O models and increase in O_3 for low N_2O models in the majority of cases. However, for our lowest O_2 levels ($\sim 0.1\%$ PAL) and the majority of M5V-hosted models, the reverse is shown. This is due to the smog mechanism of O_3 production.

4.1.3. Atmospheric chemistry. Smog mechanism efficiency and NO_x-limited and -saturated regimes

When varying the abundance of N_2O – and therefore NO_x – the smog mechanism of O₃ production becomes particularly relevant. Described in Sect. 2.1, the smog mechanism uses NO_x and HO_x as catalysts to produce O_3 in the lower atmosphere. This mechanism sources O atoms for O₃ formation from NO₂ photolysis, rather than O2 photolysis as with the Chapman mechanism. The ability for NO₂ to be photolyzed by photons spanning the NUV and into the visible spectrum is in stark contrast to 242 nm required for O₂ photolysis (see Fig. 2). Compared to the Chapman mechanism the smog mechanism can take place much deeper in the atmosphere and without the strong dependence on the host stars' NUV flux. Although smog O₃ production is increased for all high N2O cases, for the G0V-K5V hosted planets with O₂ levels of ~1% PAL and higher the destruction of O₃ via the NO_x catalytic cycle outweighs the extra smog-produced O₃ in the troposphere. However, at 0.1% PAL O₂ all cases with high N2O models show an increase in overall O3 abundance when compared to models with modern levels of N2O. This is because for low O2 levels the Chapman mechanism becomes severely limited by the amount of O₂, while the smog mechanism is less impacted as it relies on NO2 photolysis instead. However, increased O₃ smog production resulting in high O₃ abundances is evident for the M5V-hosted planet at much higher O₂ levels than other hosts, starting at 10% PAL O_2 .

There are two main reasons why the M5V-hosted planets experience a much stronger increase in smog mechanism O_3 compared to other hosts:

- the smog mechanism is much more accessible than the Chapman mechanism with lower incoming UV, as it is easier for the flux of the M5V host to photolyze NO₂ rather than O₂
- only planets hosted by the M5V star never enter the NO_x-saturated regime, meaning that the smog mechanism is not suppressed

This concept of NO_x regimes (discussed in Sect. 2.2 and demonstrated in Fig. 1) is well-illustrated in Fig. 5, in which NO and HO₂ mixing ratios for the Sun- and M5V-hosted planets are compared. Significant depletion of HO₂ is observed in parts of the atmosphere existing in the NO_x -saturated regime for the planet around the Sun. In the NO_x-limited regime, increasing NO_x allows the smog mechanism to create more O_3 , and O_3 in turn creates O(¹D) radicals that create HO_r. However, when NO_x levels are high enough to be in the NO_x-saturated regime NO_x is efficient at removing HO_x by locking it up in reservoir species (such as HNO₃ and HO₂NO₂), so an increase in NO_x leads to a decrease in HO_x. As hotter stars are more efficient at converting N_2O into NO_x – with the highest efficiency at high O_2 – NO levels become high enough to enter the NO_x -saturated regime and significantly reduce the effectiveness of the smog mechanism. For G0V-K2V hosted-planets with 100% PAL O2 all levels of N₂O explored in this study sustain high enough NO mixing ratios in parts of the lower atmosphere to be in the NO_xsaturated regime. At modern and high N2O levels parts of the atmosphere also enter the NO_x-saturated regime for the G0V-, Sun-, and K2V- hosted planets at 10% PAL O₂, as well the G0V and Sun cases slightly at 1% PAL O₂. On the other hand, the low UV flux of the M5V host star struggles to convert N_2O into NO_x , consistently keeping it in the NO_x -limited regime and allowing for a boost in smog O₃ production whenever N₂O is increased.

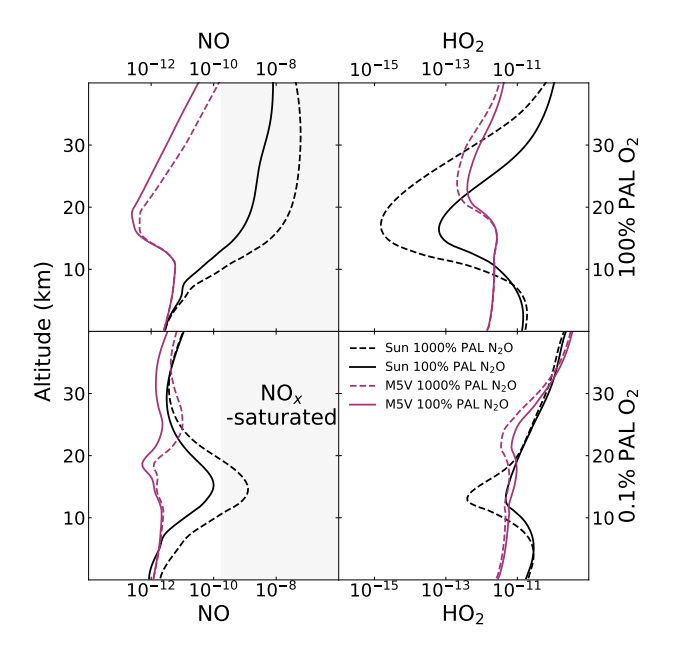


Fig. 5. NO and HO₂ profiles at 100 and 0.1% PAL O₂ for planets around the Sun and M5V hosts. Plots containing NO profiles indicate the NO_x-saturated regime by a gray background, while the NO_x-limited regime has a white background. When NO profiles enter the NO_x-saturated regime, a corresponding depletion of HO₂ appears in the same part of the atmosphere. The Sun-hosted planet often enters the NO_x-saturated regime, due to the efficient conversion of N₂O into NO_x. By contrast, the M5V-hosted planet is less efficient at creating NO_x in its low UV environment and remains in the NO_x-limited regime.

4.2. UV to ground

This section explores how the changes in the O₂-O₃ relationship translate to changes in the surface UV environment when varying N2O. On modern Earth both O2 and O3 are very important for UV shielding, which is important for surface life to flourish. Although O₂ is not as efficient at shielding UV as O₃ (see a comparison of absorption cross sections in Fig. 2), it is significantly more abundant than O₃, and thus being a large constituent of our atmosphere it provides significant shielding. We discuss surface UV environments using three biological regimes of UV: UVA (315-400 nm) is least damaging and may help power complex processes necessary for life; UVB (280–315 nm), which is more dangerous and has been linked to tanning of skin as well as skin cancer; and UVC (121.6-280 nm), which is dangerous for biological organisms and can break apart DNA. On modern Earth UVA is not largely shielded by O₃ or O₂, UVB is partially shielded by O₃, and fortunately UVC is almost entirely shielded by O₂ and O₃, protecting surface life. UVB and particularly UVC have a nonlinear relationship with the amount of O_2/O_3 , and are very sensitive to changes in O_3 . See Kozakis et al. (2022) for an in-depth description of the impacts of UV on the ground while varying only O₂. Comparisons of the top-of-theatmosphere (TOA) and integrated UVC surface flux (the most variable results) are shown in Fig. 6, with an additional table in the appendix (Table A.1) displaying absolute and normalized UVB and UVC surface fluxes. UVA results were unaffected when changing N_2O , with all models allowing ~80% of incoming UVA to reach the surface, as in Kozakis et al. (2022). This is unsurprising as O_3 does not provide shielding at these wavelengths, with other species causing minimal absorption.

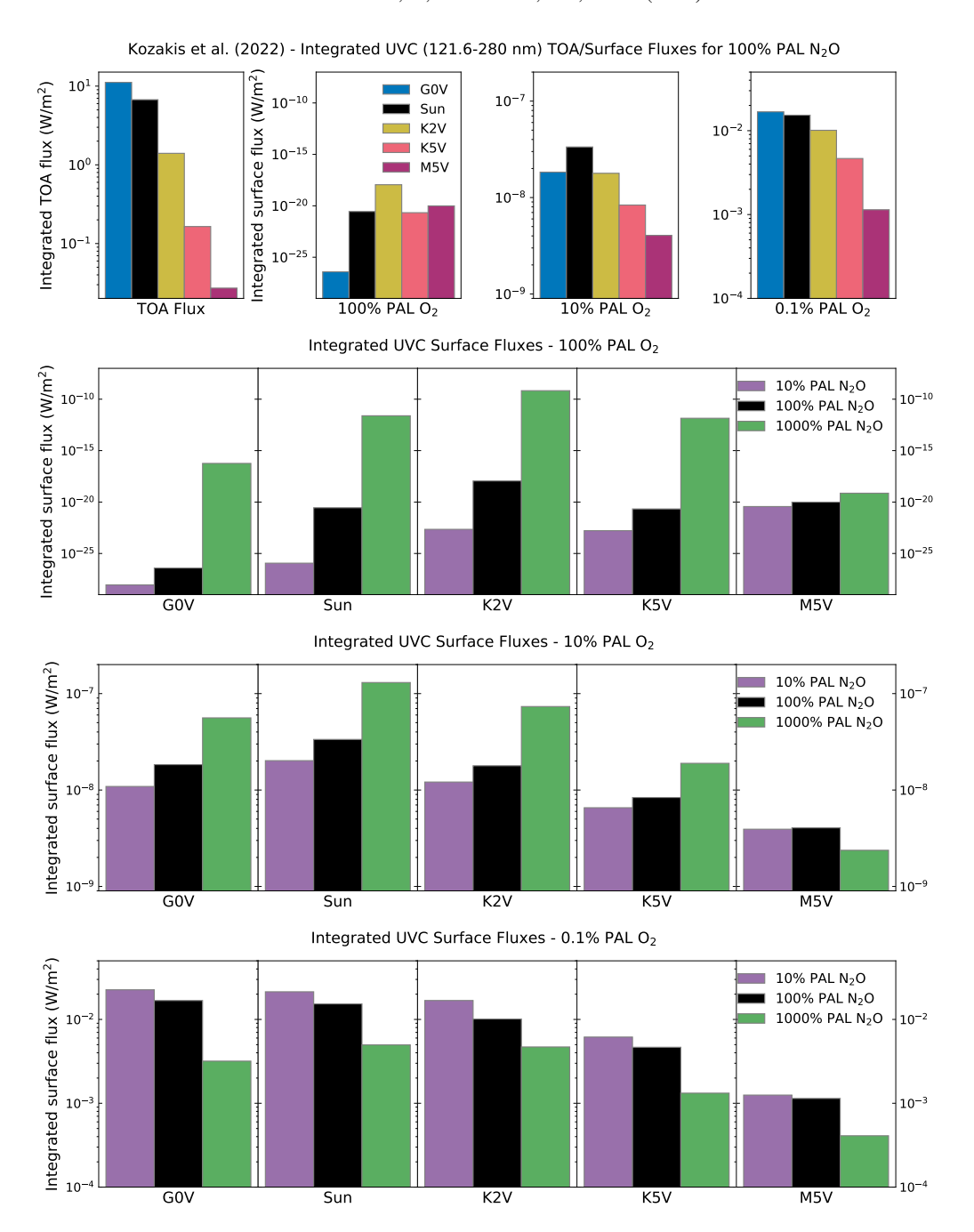


Fig. 6. UVC surface fluxes for planets around all hosts from Kozakis et al. (2022) with modern N_2O (top) and with high and low N_2O abundances from this study with O_2 levels of 100% (second row), 10%, (third row), and 0.1% (bottom) PAL. The first panel in the top row indicates the top-of-the-atmosphere (TOA) flux for planets around all host stars, with the rest of the top row using the same y-axis limits for the corresponding O_2 values used in the bottom three rows to facilitate comparisons. Results for 1% PAL O_2 are extremely similar to those for 10% PAL O_2 and are therefore not included. The most significant changes in UVC surface flux occur in models with higher O_2 because the conversion from O_2 0 to O_2 1 is more efficient in higher O_2 2 environments. Larger amounts of O_2 4 have a greater impact on O_3 6 either by depleting it with O_2 6 catalytic cycles or producing it with the smog mechanism. While the results at O_2 6 and O_2 7 then to show increased O_3 6 shielding for low O_3 7 models, this trend reverses at O_3 7 PAL O_3 7, where the low O_3 8 models consistently receive more surface UVC. This is because at low O_3 8 levels the effects of the smog mechanism become clearer as the Chapman mechanism is limited by the lack of O_3 8.

UVB surface flux displays more variation when changing levels of N_2O , but always within an order of magnitude. Higher O_2 levels allow larger variations in UVB surface fluxes, as there are typically higher O_3 levels, resulting in greater absolute changes in O_3 abundance and UV shielding ability. The high N_2O models showed the largest change in surface UVB flux at high O_2 levels as increased efficiency of the NO_x catalytic cycle caused significant changes in O_3 for planets around all hosts

except for the M5V. The most variation was at 100% PAL O_2 for the G0V-hosted planet with 1.8 times as much UVB flux reaching the surface for the high N_2O models, and 0.72 times as much flux reaching the surface for low N_2O models. The only planet not experiencing large changes in UVB surface flux at these O_2 levels for varying N_2O cases was the one hosted by the M5V star, as the low UV flux did not allow efficient conversion of N_2O into NO_x , and did not impact O_3 abundance as much as other hosts.

The most significant changes in the UV surface environment were for the UVC surface flux as it covers the wavelength range in which O₃ shielding is most effective, causing O₃ changes from varying N2O to strongly impact UVC surface flux. Similarly to UVB surface flux, for all but the planet hosted by the M5V star, the largest changes in UVC surface flux were caused by the high N₂O cases at higher O₂ levels. This was due once again to the significantly increased efficiency of the NO_x catalytic cycle with increased NO_x sourced from N₂O. The largest increase was observed for the G0V-hosted planet with the high N₂O model at 100% PAL O₂, which experienced an astounding 15 billion-fold increase in UVC surface flux. However, even with this extreme increase in surface UVC flux this case still experiences less surface UVC flux than planets around all other hosts except the M5V for the high N₂O models at this O₂ level. This is because initially the GOV-hosted planet had the strongest UVC shielding at 100% PAL O₂ due to having the highest O₃ abundance. The ability of the high N₂O models to deplete O₃ with sufficient O₂ is still seen at the 10% PAL O₂ level where there were still significant increases in surface UVC flux for planets around all hosts except for the M5V, which had less surface UVC due to increased amounts of smog produced O₃ around hosts with lower UV. For our lowest O₂ levels planets around all hosts start to show decreased levels of UVC surface flux for the high N₂O models compared to modern levels of N₂O due to the extra UV shielding from the O₃ produced by the smog mechanism.

The largest reduction of UVC surface flux from the low N_2O models was observed for the Sun-hosted planet, with a factor of 4.1×10^{-6} times the original UVC surface flux with modern N_2O at 100% PAL O_2 , due to a less productive NO_x catalytic cycle. From the high N_2O models the largest UVC surface flux reduction was observed for the planet around the G0V host at 0.1% PAL O_2 , with only a factor of 0.19 UVC flux reaching the surface compared to modern N_2O levels due to extra O_3 from smog production. Overall the N_2O models with the least UVC surface flux variation were those around the M5V host, due largely to the fact that these cases had the least amount of total O_3 , so the absolute amount of surface flux does not have much variation.

4.3. Planetary emission spectra

In this section we examine how the effects of N₂O on the O₂-O₃ relationship would impact potential future observations. We focus in particular on the 9.6 µm O₃ feature to see how it would change for different N2O abundances. Already in Kozakis et al. (2022) we found that just varying levels of O₂ results in counterintuitive changes in the depth of the O₃ spectral feature. This is due to the fact that spectral feature depth for emission spectra is dependent on not only the abundance of O₃, but also the temperature difference between the absorbing and emitting layers of the atmosphere. This causes a nonlinear relationship between O₃ abundance and feature depth as O₃ has a significant impact on stratospheric heating. Ozone absorption features for planets with significant stratospheric heating will be shallower due to a decreased temperature difference between the stratosphere and surface when compared to a planet with less O₃ and less stratospheric heating. This effect impacts planets around hotter stars more than those around cooler stars, as O₃ heats the atmosphere via absorption of NUV photons and cooler stars (especially M dwarfs) have less NUV flux due lower temperatures and TiO absorption. Since the atmospheres of planets around cooler stars tend to be more isothermal, spectral feature depth has a more linear relationship between O₃ abundance and O₃ feature depth, as

seen in the left-hand side of Fig. 7, which displays emission spectra from Kozakis et al. (2022). For a more in-depth look at how this effect impacts O₃ spectral features with varying O₂ levels please refer to Kozakis et al. (2022).

Figure 7 shows 9.6 µm O₃ features with varying N₂O normalized to features with modern levels of N2O in order to understand how observations of O₃ could be impacted by varying N₂O abundances. When comparing model atmospheres with varying N₂O to those with modern levels of N₂O, the largest changes in temperature profiles (and, therefore, the spectral features) were due to changing amounts of stratospheric heating from O_3 , which often was not a large change. As a result, changes in the O₃ feature depth were due primarily to variations in O₃ abundance, rather than the atmospheric temperature profile as in Kozakis et al. (2022). Overall the most significant changes in spectral feature strength were caused by the high N₂O models at higher O₂ levels, which is unsurprising as these are the cases with the largest depletion in O₃ from the enhanced NO_x catalytic cycle. The planet around the K2V host at 100% PAL O₂ with the high N₂O model has the spectral feature that changes the most compared to modern levels of N2O, with a shallower feature caused by O₃ depletion. At 0.1% PAL O₂ for planets around all hosts there is a deeper O₃ feature due to the extra O₃ produced by the smog mechanism at low levels of O₂. There is less variation in spectral feature strength for the low N2O models as they had a much weaker effect on O₃.

5. Discussion

5.1. Comparisons to other studies

Here we discuss studies examining how changes in N_2O would impact a planet, especially with different O_2 and O_3 levels. For a full review of studies exploring the relationship between O_2 and O_3 , see Kozakis et al. (2022). While no other study varied N_2O specifically to look at changes in the O_2 - O_3 relationship, there exist studies similar enough that it is useful to compare trends.

Grenfell et al. (2006) explores the possibility that on early Earth during periods with low O_2 , O_3 produced by the smog mechanism using NO_2 photolysis instead of O_2 photolysis could have provided UV shielding for surface life. Motivated by the fact that HO_x levels and possibly N_2O levels were higher during the Proterozoic period (2.4–0.54 Gyr ago), they varied CH_4 , O_2 , NO_x , H_2 , and CO abundances to study the impact on smog O_3 formation using a photochemistry box model. Although they explore a different parameter space than in this study, similar trends appear, and they also see the effects of the atmosphere in a NO_x -saturated regime, which suppresses O_3 formation, similarly to what we find at high N_2O in our model atmospheres around the hotter stars.

There are also several studies in a similar vein focusing on planets in M dwarf systems, especially since the low incoming UV from such hosts could lead to a buildup of N_2O in their atmospheres (Segura et al. 2003, 2005). Rauer et al. (2011) and Grenfell et al. (2013) – both part of the same paper series – discuss the increased smog production efficiency of planets around M dwarfs, particularly late-type M dwarfs. This idea is explored in depth in Grenfell et al. (2013), where they use the Pathway Analysis Program (Lehmann 2004) to compare the efficiencies of the Chapman and smog mechanisms of O_3 production. Although they use an earlier version of Atmos for their atmospheric modeling, they utilize a more complex chemical network to study smog formation, including variations of the smog mechanism that are not included in our chemical network

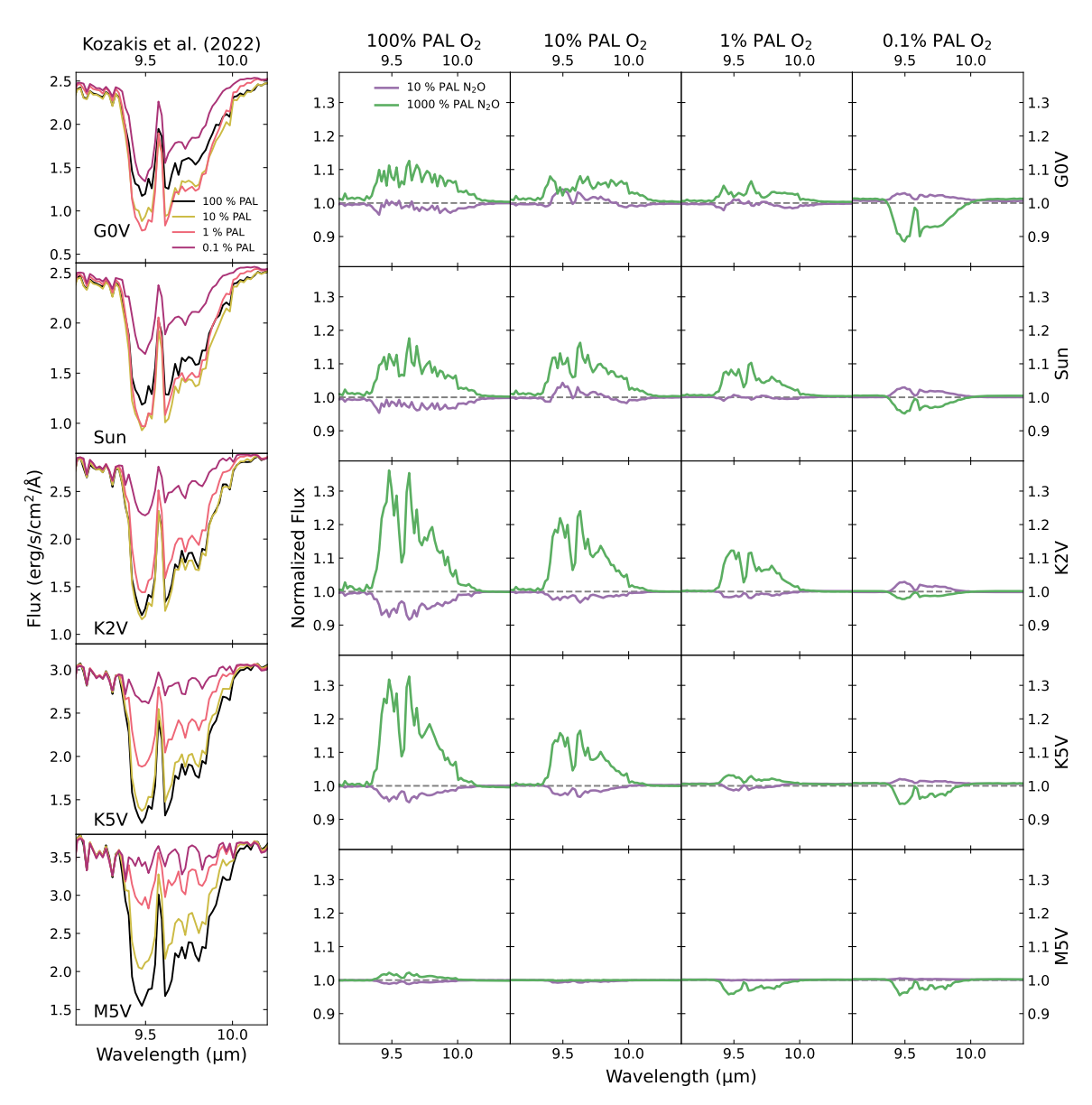


Fig. 7. 9.6 μ m O_3 feature for models from Kozakis et al. (2022) (left) and normalized models from varying N_2O (right) from simulated planetary emission spectra. Changes in the O_3 feature for this study depended primarily on changes in O_3 abundance – rather than on changes in the atmospheric temperature profile, as in Kozakis et al. (2022) – since varying N_2O often did not significantly impact the temperature profiles. As the K5V-hosted planet experienced the greatest change in O_3 abundance with the high N_2O models, it follows that its O_3 emission spectral features were the most impacted. The M5V-hosted planet experienced the smallest change in O_3 while varying N_2O , which is reflected by the small variations in its O_3 feature.

that involve more complex methyl-containing molecules (e.g., CH_3O_2). However, the "classical" smog mechanism that we use in this study is shown to be the most common type of smog production. The trends reported in Grenfell et al. (2013) agree with those discussed in this study, especially with our results for increased smog production of O_3 around our coolest host, the M5V. However, Grenfell et al. (2013) do not vary O_2 or N_2O abundances. Another study, Grenfell et al. (2014), varies N_2O and CH_4 biological surface fluxes, along with incoming UV fluxes to explore the effect of a planet orbiting an M7V host star. Although they use an M7V host star and explore different N_2O abundances than in this paper (N_2O at a factor of 1000 lower and zero N_2O flux), similar trends are observed – particularly decreased smog production for decreased N_2O , which we see especially in our models around cooler host stars.

Schwieterman et al. (2022) explores what a plausible range of N_2O surface fluxes could be for terrestrial planets using both a biogeochemical model and a photochemistry model (from Atmos). Using the biogeochemical model cGENIE they predict possible N_2O surface fluxes based off denitrification process at O_2 abundances from 1–100% PAL with planet hosts ranging from F2V to M8V. By modeling total ocean denitrification they determine maximum N_2O atmospheric mixing ratios for different O_2 abundances. Their results show that our high N_2O models (using an N_2O mixing ratio of 3 ppm) are safely within the range of possible N_2O values for all spectral host types. Although Schwieterman et al. (2022) also explores atmospheres with different amounts of N_2O and O_2 as in our study, the focus is not on O_3 so it is difficult to make direct comparisons. Schwieterman et al. (2022) briefly show that increasing N_2O

results in increased destruction of stratospheric O_3 , agreeing with our general results, although they do not discuss if increased smog mechanism formation occurs at large N_2O values. Overall, when comparing our current study to other similar works there appears to be no real inconsistencies, although the studied parameter spaces are varied enough that it is not possible to make direct comparisons.

5.2. Plausible N2O mixing ratios in Earth-like atmospheres

In this study we used fixed mixing ratio profiles for N₂O to facilitate comparisons of how those levels of N₂O were expected to impact the O₂-O₃ relationship across different host stars. However, it is important to recognize that the relationship between surface flux and resulting atmospheric mixing ratios is not linear, and is highly influenced by the host star as well as atmospheric content. For N₂O in particular the O₂ level has significant impact on the resulting mixing ratio, meaning that there would be a range of N₂O fluxes that would be necessary to reproduce the mixing ratios used in this study. As stated in Sect. 3, the motivation behind our chosen N₂O abundances is to begin filling in the parameter space of how atmospheric variations impact the O₂-O₃ relationship. Using such a large range of N₂O allows us to understand in which scenarios we would expect O₃ abundances to be impacted in a way that would make observations more difficult to interpret. We briefly review expected N₂O surface fluxes over time, and atmospheric parameters impact their mixing ratios.

As alluded to earlier, abundances of N₂O can be strongly impacted by O₂ abundances due primarily to UV shielding and reactions with O₂ and oxygen-containing species. In addition, the level to which N2O can buildup in an atmosphere is also dependent on the host star, with cooler stars allowing for more buildup in their atmospheres due to lower incoming UV fluxes (e.g., Segura et al. 2003, 2005). As mentioned during the previous subsection, with N2O there has been work done to evaluate the maximum possible surface fluxes and corresponding mixing ratios using biogeochemical and photochemistry models (Schwieterman et al. 2022). It is also more complicated to evaluate these limits, since O₂ influences both the surface flux and mixing ratio of N₂O. The production of N₂O surface flux is caused by nitrification and denitrification processes, whereas N₂O mixing ratios depend on N₂O destruction rates via photolysis and O(¹D) radicals in the stratosphere. For both surface flux and atmospheric mixing ratios, the dependence on O2 is complicated, as nitrification processes require O2 and denitrification processes require an absence of O2. Moreover, while O2 also creates O₃, which protects atmospheric N₂O from photolysis, increased O₂ also causes increased O(¹D) radicals – another major sink for N2O. Additionally, due to the dependency on incoming UV, the amount of N₂O in the atmosphere is highly influenced by the host star, requiring careful modeling.

It is possible that N_2O surface fluxes were much higher in the past, particularly during the Proterozoic era. On modern Earth the majority of denitrification processes end with N_2O being converted into N_2 , but this conversion requires a metal catalyst, most commonly Copper (see Schwieterman et al. 2022 for details). However during the Proterozoic era it is estimated that the oceans were highly depleted of Copper (Saito et al. 2003; Zerkle et al. 2006; Roberson et al. 2011), potentially causing significantly higher N_2O fluxes as N_2O would not be converted into N_2 . Although, for planets around hotter stars like the Sun in order not to have widespread depletion of N_2O via photolysis, O_2 levels of about 10% PAL would be necessary to provide UV

shielding (Roberson et al. 2011). If so, N₂O could have accumulated on Proterozoic Earth to levels high enough to contribute to warming during this time period.

6. Summary and conclusions

This study focuses on how varying N_2O abundances in the atmosphere of an Earth-like planet impact the O_2 - O_3 relationship across a range of O_2 levels around a variety of host stars. We find that the impact of varying N_2O depends on both the host star and the amount of O_2 in the atmosphere (see Fig. 3). Adding additional N_2O to an atmosphere rather than removing it consistently yielded more significant changes to O_3 formation and destruction.

Atmospheric chemistry for models with varying N2O (Sect. 4.1) show that, for O₂ levels greater than 1% PAL, planets around all hosts except the M5V experience significant depletion in O₃ in the high N₂O models compared to modern levels of N₂O, due to the enhanced efficiency of the NO_x catalytic cycle. Planets around the M5V hosts are the least impacted by this effect, due to their low-incoming UV flux having a weakened ability to convert N_2O into NO_x . However, the M5V-hosted planets were most efficient at creating extra O₃ at high N₂O with the smog mechanism in the lower atmosphere, especially at lower O2 levels as the low UV environment was more suited to NO₂ photolysis than O₂ photolysis. At O₂ levels of 0.1% PAL and lower, planets around all hosts experienced an increase in O₃ with the high N₂O models. This was due to the more dominant effects of the smog mechanism, as the Chapman mechanism was extremely limited by low O₂. However, the increase was not as pronounced as that seen for the planet around the M5V host. This is because the higher efficiency of hotter stars in converting N₂O into NO_x resulted in NO_x abundances high enough to reach the NO_x -saturated regime, thereby suppressing O_3 smog formation.

The UV flux reaching the surface of our model planets was impacted by the changes in O₃ (Sect. 4.2) especially since O₃ abundance and attenuation of UV in the atmosphere have a nonlinear relationship. Results for the UVC surface flux are shown in Fig. 6, as this wavelength range is not only the most dangerous for life, but also the most sensitive to changes in O₃. The most extreme example of changing UVC surface flux was observed for the G0V-hosted planet at modern levels of O_2 and high N_2O , which received a 15 billion-fold increase in UVC ground flux compared to modern levels of N₂O. For planets around all the hosts except the M5V, the largest changes in UVC at the surface occurred in the high N2O cases. More flux reached the surface at O_2 levels above 0.1% PAL due to NO_x destroying O_3 , while less UV reached the ground in low O₂ cases of 0.1% PAL because of additional UV shielding from O₃ produced by the smog mechanism. However, for the high N₂O models around the M5V host, there was greater UV shielding at O₂ levels of 10% PAL and below, due to the increased O₃ formed by the smog mechanism.

Lastly, we explored how changing N_2O abundances could potentially impact O_3 measurements in future observations and the ability to use O_3 to learn about the amount of O_2 in a planetary atmosphere (Sect. 4.3). We focused particularly on the 9.6 μ m O_3 feature for the simulated planetary emission spectra and how the feature would change with different abundances of N_2O (Fig. 7). Unlike in Kozakis et al. (2022), changes in feature depth were influenced more by changes in O_3 than by temperature profiles. While decreasing the amount of N_2O had little impact on the O_3 feature, increasing it had a significantly larger impact. The destruction of O_3 for hotter hosts at high O_2 levels particularly influenced the feature depth, resulting in shallower

features, with the K5V-hosted planet being the most impacted. The planet around the M5V dwarf only had significant changes in the $\rm O_3$ feature for the high $\rm N_2O$ models at low $\rm O_2$ levels, due to the amount of extra $\rm O_3$ produced by the smog mechanism in the lower atmosphere.

When considering this work in the context of planning future observations, no host star displayed results showing that O_3 measurements in the mid-IR would be unaffected by the abundance of N_2O in their atmospheres. We propose that a separate measurement of N_2O is important for using O_3 to assess the abundance of O_2 in an atmosphere. Fortunately, if we consider mid-IR measurements once again, there exists a N_2O feature, albeit overlapping with a CH_4 feature, potentially causing data interpretation issues. A variety of studies have been carried out in preparation for future observations of the proposed LIFE mission in the mid-IR (e.g., Konrad et al. 2022; Alei et al. 2022; Konrad et al. 2023; Alei et al. 2024; Angerhausen et al. 2024); however, more in-depth studies focusing on the different levels of N_2O would be helpful in the pursuit of using O_3 as a means to learn about potential life on a terrestrial exoplanet.

Studying the O_2 - O_3 relationship in the context of varying N_2O abundances reveals another layer of complexity in addition to what we already find in Kozakis et al. (2022). As with all atmospheric measurements of terrestrial exoplanets, context will be essential for truly understanding the meaning of our observations. This work further reinforced the idea that understanding the host star is necessary to understand the planet. It also highlights the need to measure additional atmospheric species before using O_3 as a way to infer biologically produced O_2 and the potential for surface life on a planet.

Acknowledgements. All computing was performed on the HPC cluster at the Technical University of Denmark (DTU Computing Center 2021). This project is funded by VILLUM FONDEN. Authors TK and LML acknowledge financial support from the Severo Ochoa grant CEX2021-001131-S funded by MCIN/AEI/10.13039/501100011033. JMM acknowledges support from the Horizon Europe Guarantee Fund, grant EP/Z00330X/1. We thank the anonymous referee for providing comments, which improved the clarity of our manuscript.

References

```
Alei, E., Konrad, B. S., Angerhausen, D., et al. 2022, A&A, 665, A106
Alei, E., Quanz, S. P., Konrad, B. S., et al. 2024, A&A, 689, A245
Angerhausen, D., Pidhorodetska, D., Leung, M., et al. 2024, AJ, 167, 128
Arney, G., Domagal-Goldman, S. D., Meadows, V. S., et al. 2016, Astrobiology, 16, 873
Batalha, N. E., Marley, M. S., Lewis, N. K., & Fortney, J. J. 2019, ApJ, 878, 70
Batalha, N., Rooney, C., & MacDonald, R. 2021, https://doi.org/10.5281/zenodo.5093710
Braam, M., Palmer, P. I., Decin, L., et al. 2022, MNRAS, 517, 2383
Chapman, S. A. 1930, Mem. R. Met. Soc., 3, 103
Des Marais, D. J., Harwit, M. O., Jucks, K. W., et al. 2002, Astrobiology, 2, 153
DTU Computing Center 2021, DTU Computing Center resources
```

```
Fauchez, T. J., Villanueva, G. L., Schwieterman, E. W., et al. 2020, Nat. Astron.,
France, K., Loyd, R. O. P., Youngblood, A., et al. 2016, ApJ, 820, 89
Gregory, B. S., Claire, M. W., & Rugheimer, S. 2021, Earth Planet. Sci. Lett.,
   561, 116818
Grenfell, J. L., Stracke, B., Patzer, B., Titz, R., & Rauer, H. 2006, Int. J.
   Astrobiol., 5, 295
Grenfell, J. L., Gebauer, S., Godolt, M., et al. 2013, Astrobiology, 13, 415
Grenfell, J. L., Gebauer, S., v. Paris, P., Godolt, M., & Rauer, H. 2014,
  Planet, Space Sci., 98, 66
Haagen-Smit, A. J. 1952, Ind. Eng. Chem., 44, 1342
Harman, C. E., Schwieterman, E. W., Schottelkotte, J. C., & Kasting, J. F. 2015,
   ApJ, 812, 137
Kasting, J. F. 1979, PhD thesis, University of Michigan, United States
Kasting, J. F., & Ackerman, T. P. 1986, Science, 234, 1383
Kasting, J. F., Holland, H. D., & Pinto, J. P. 1985, J. Geophys. Res. 90, 10497
Kitzmann, D., Patzer, A. B. C., von Paris, P., Godolt, M., & Rauer, H. 2011,
Konrad, B. S., Alei, E., Quanz, S. P., et al. 2022, A&A, 664, A23
Konrad, B. S., Alei, E., Quanz, S. P., et al. 2023, A&A, 673, A94
Kopparapu, R. K., Ramirez, R., Kasting, J. F., et al. 2013, ApJ, 770, 82
Kozakis, T., Mendonça, J. M., & Buchhave, L. A. 2022, A&A, 665, A156
Kump, L. 2008, Nature, 451, 277
Kurucz, R. L. 1979, ApJS, 40, 1
Lederberg, J. 1965, Nature, 207, 9
Léger, A., Fontecave, M., Labeyrie, A., et al. 2011, Astrobiology, 11, 335
Lehmann, R. 2004, J. Atmos. Chem., 47, 45
Lippincott, E. R., Eck, R. V., Dayhoff, M. O., & Sagan, C. 1967, ApJ, 147,
Logan, J. A., Prather, M. J., Wofsy, S. C., & McElroy, M. B. 1981, J. Geophys.
   Res.: Oceans, 86, 7210
Lovelock, J. E. 1965, Nature, 207, 568
Léger, A., Pirre, M., & Marceau, F. J. 1993, A&A, 277, 309
Meadows, V. S. 2017, Astrobiology, 17, 1022
Meadows, V. S., Arney, G. N., Schwieterman, E. W., et al. 2018a, Astrobiology,
   18, 133
Meadows, V. S., Reinhard, C. T., Arney, G. N., et al. 2018b, Astrobiology, 18,
Nicolet, M. 1975, Planet. Space Sci., 23, 637
Quanz, S. P., Absil, O., Benz, W., et al. 2022, Experimental Astronomy, 54, 1197
Ratner, M. I., & Walker, J. C. G. 1972, J. Atmos. Sci., 29, 803
Rauer, H., Gebauer, S., Paris, P. V., et al. 2011, A&A, 529, A8
Roberson, A. L., Roadt, J., Halevy, I., & F., K. J. 2011, Geobiology, 9, 313
Rugheimer, S., Kaltenegger, L., Segura, A., Linsky, J., & Mohanty, S. 2015, ApJ,
   809, 57
Saito, M. A., Sigman, D. M., & Morel, F. M. 2003, Inorg. Chim. Acta, 356, 308
Schwieterman, E. W., Kiang, N. Y., Parenteau, M. N., et al. 2018, Astrobiology,
Schwieterman, E. W., Olson, S. L., Pidhorodetska, D., et al. 2022, ApJ, 937, 109
Segura, A., Krelove, K., Kasting, J. F., et al. 2003, Astrobiology, 3, 689
Segura, A., Kasting, J. F., Meadows, V., et al. 2005, Astrobiology, 5, 706
Shumilov, O. I., Kasatkina, E. A., Turyansky, V. A., Kyro, E., & Kivi, R. 2003,
   Adv. Space Res., 31, 2157
Teal, D. J., Kempton, E. M. R., Bastelberger, S., Youngblood, A., & Arney, G.
  2022, ApJ, 927, 90
Toon, O. B., McKay, C. P., Ackerman, T. P., & Santhanam, K. 1989, J. Geophys.
  Res., 94, 16287
```

Tuck, A. F. 1976, Q. J. Roy. Meteorol. Soc., 102, 749

285

Zahnle, K., Claire, M. W., & Catling, D. 2006, Geobiology, 4, 271

Zerkle, A. L., House, C. H., COX, R. P., & Canfield, D. E. 2006, Geobiology, 4,

Appendix A: Supporting figures and tables

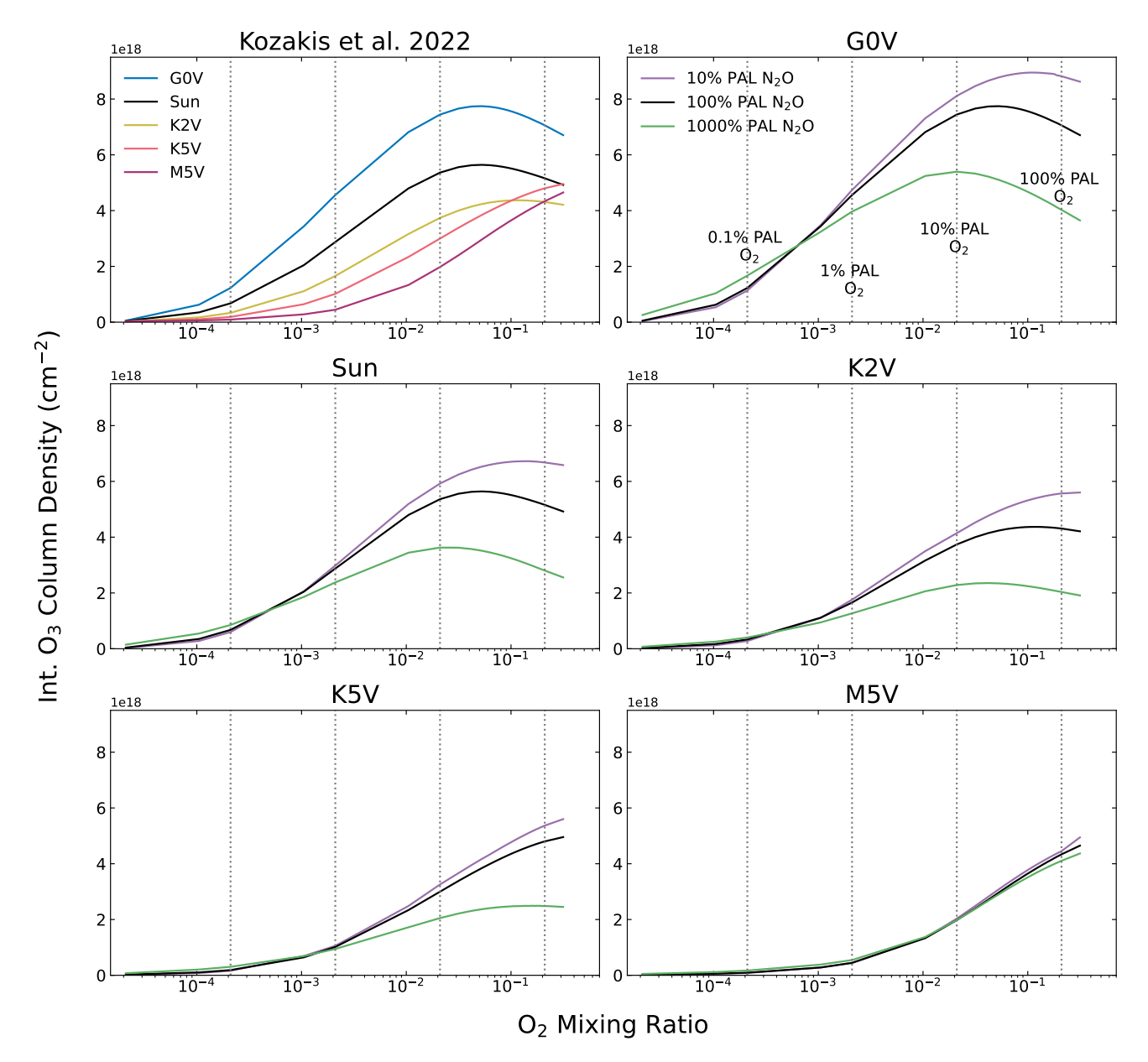


Fig. A.1. O_2 - O_3 relationship for changing N_2O , along with models from Kozakis et al. (2022) for comparison, for all modeled O_2 mixing ratios. Vertical dashed lines indicate O_2 levels of 100%, 10%, 1%, and 0.1% PAL. All plots share the same y-axis to facilitate comparison between different host stars. The phenomena that causes the peak O_3 value for GoV-, Sun-, and K2V-hosted planets to occur at O_2 levels less than the maximum value modeled (150% PAL O_2) is discussed at length in Kozakis et al. (2022).

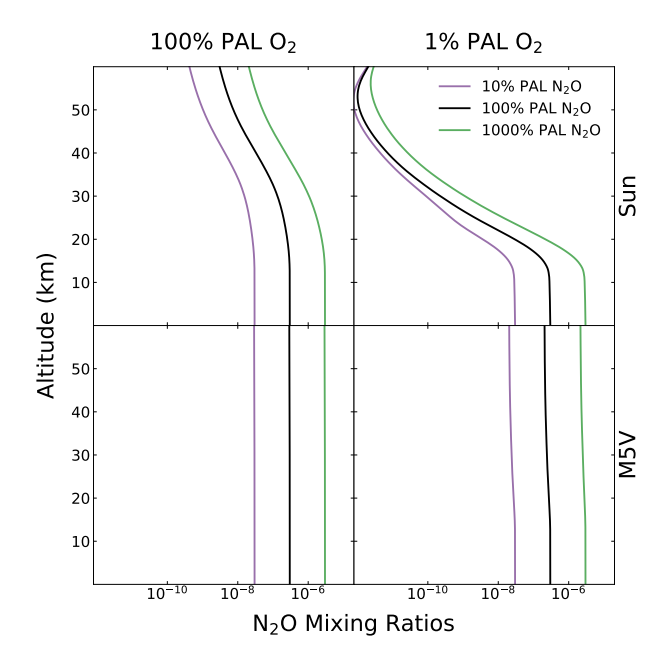


Fig. A.2. N_2O profiles for planets around the Sun and M5V hosts at 100% and 1% PAL O_2 . The sun-hosted planet shows significant amounts of N_2O depletion via photolysis (the main stratospheric sink of N_2O), especially at lower O_2 levels, as the UV protection from both O_2 and O_3 is significantly lessened. This depletion of N_2O impacts the conversion of N_2O to NO_x . Meanwhile, the M5V-hosted planet experiences very little photolysis at all O_2 levels, due to the low UV flux of the host star.

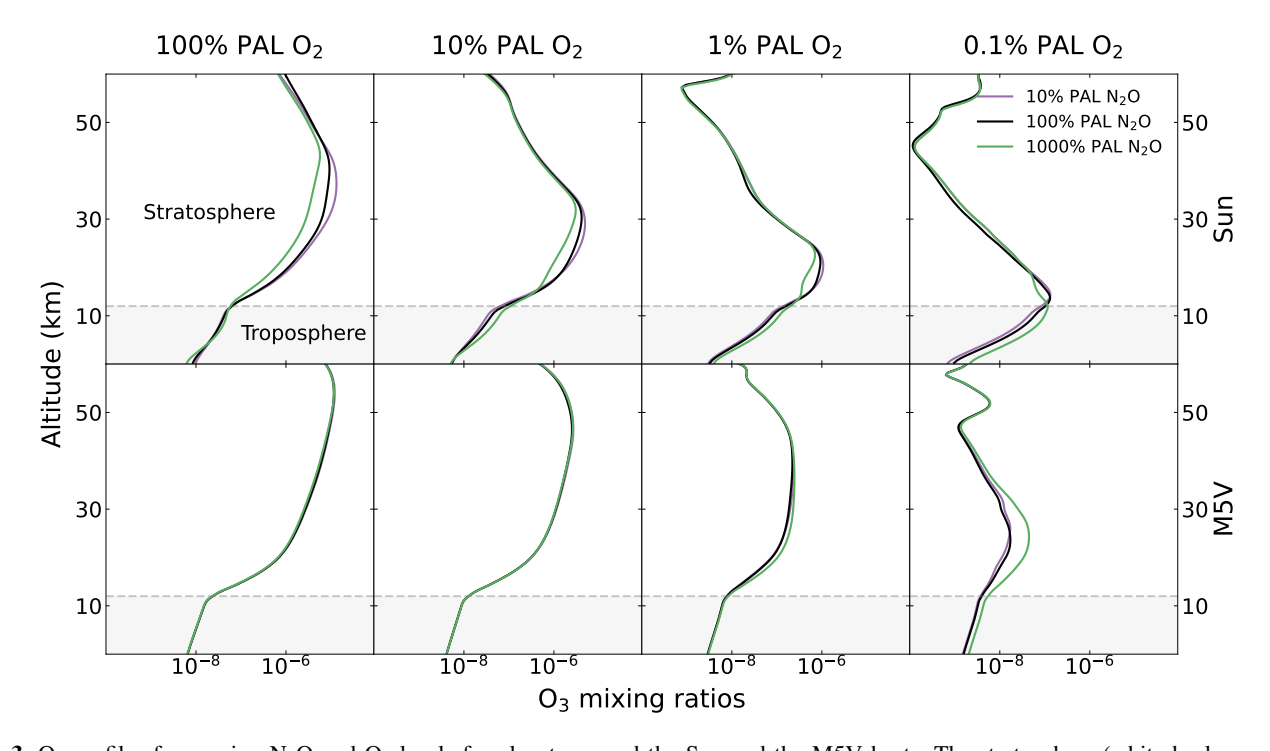


Fig. A.3. O_3 profiles for varying N_2O and O_3 levels for planets around the Sun and the M5V hosts. The stratosphere (white background) and troposphere (gray background) are indicated in order to draw attention to differences in O_3 production and depletion with the two stellar hosts. While at higher O_2 levels the Sun-hosted planet efficiently destroys stratospheric O_3 , the M5V-hosted planet experiences minimal stratospheric O_3 depletion at all O_2 levels. The smog mechanism dominates in the lower atmosphere for the two hosts, especially at lower O_2 , but it is restricted to the troposphere for the planet around the Sun. Smog O_3 is produced into the stratosphere for the planet around the M5V host, due to the lack of suppression the Sun-hosted planet experiences in the NO_x -saturated regime. See Figs. 1 and 5 for more information on the NO_x -limited and NO_x -saturated regimes.

Table A.1. UV Integrated Fluxes

Spectral	O ₂ MR	TOA flux	Kozakis et al. (2022)	Surface Flux Normaliz	ed to Kozakis et al. (2022)
Type	(% PAL)	(W/m^2)	Surface Flux (W/m ²)	10% PAL N ₂ O	1000% PAL N ₂ O
UVB Fluxes (280–315 nm)					
G0V	100	22.35	1.5e+00	0.72	1.84
G0V	10	22.35	1.4e+00	0.88	1.47
G0V	1	22.35	2.4e+00	0.97	1.13
G0V	0.1	22.35	5.9e+00	1.05	0.84
Sun	100	16.18	1.6e+00	0.74	1.69
Sun	10	16.18	1.6e+00	0.89	1.43
Sun	1	16.18	2.7e+00	0.98	1.13
Sun	0.1	16.18	5.6e+00	1.05	0.90
K2V	100	4.8	6.8e-01	0.79	1.67
K2V	10	4.8	7.4e-01	0.92	1.39
K2V	1	4.8	1.2e+00	0.97	1.13
K2V	0.1	4.8	2.2e+00	1.04	0.95
K5V	100	0.68	9.8e-02	0.90	1.60
K5V	10	0.68	1.4e-01	0.95	1.24
K5V	1	0.68	2.3e-01	0.99	1.02
K5V	0.1	0.68	3.4e-01	1.02	0.92
M5V	100	3.5e-02	6.5e-03	0.98	1.04
M5V	10	3.5e-02	1.0e-02	0.99	1.00
M5V	1	3.5e-02	1.6e-02	1.00	0.96
M5V	0.1	3.5e-02	2.0e-02	1.01	0.94
UVC Fluxes (121.6–280 nm)					
G0V	100	11.2	3.8e-27	2.3e-02	1.5e+10
G0V	10	11.2	1.8e-08	5.9e-01	3.1e+00
G0V	1	11.2	1.7e-04	1.0e+00	5.2e-01
G0V	0.1	11.2	1.7e-02	1.3e+00	1.9e-01
Sun	100	6.7	2.8e-21	4.1e-06	8.8e+08
Sun	10	6.7	3.3e-08	6.0e-01	3.9e+00
Sun	1	6.7	2.3e-04	1.0e+00	7.2e-01
Sun	0.1	6.7	1.5e-02	1.4e+00	3.2e-01
K2V	100	1.4	1.1e-18	2.0e-05	6.0e+08
K2V	10	1.4	1.8e-08	6.8e-01	4.1e+00
K2V	1	1.4	1.0e-04	9.8e-01	8.4e-01
K2V	0.1	1.4	1.0e-02	1.7e+00	4.6e-01
K5V	100	0.16	2.1e-21	7.8e-03	6.6e+08
K5V	10	0.16	8.4e-09	7.8e-01	2.3e+00
K5V	1	0.16	5.4e-05	1.0e+00	5.7e-01
K5V	0.1	0.16	4.7e-03	1.3e+00	2.8e-01
M5V	100	2.7e-02	9.8e-21	3.7e-01	7.4e+00
M5V	10	2.7e-02	4.1e-09	9.7e-01	5.9e-01
M5V	1	2.7e-02	3.8e-05	1.0e+00	4.0e-01
M5V	0.1	2.7e-02	1.1e-03	1.1e+00	3.6e-01

Notes. Abbreviations: MR = mixing ratio; PAL = present atmospheric level; TOA = top of atmosphere